Investigating Tau and Amyloid Tracer Skull Binding in Studies of Alzheimer Disease

Shaney Flores[1], Charles D. Chen[1], Yi Su[2], Aylin Dincer[1], Sarah J. Keefe[1], Nicole S. McKay[1], Angela M. Paulick[1], Gloria Guzman Perez-Carrillo[1], Liang Wang[1], Russ C. Hornbeck[1], Manu Goyal[1,3,4], Andrei Vlassenko[1,3], Sally Schwarz[1], Michael L. Nickels[1], Dean F. Wong[1], Zhude Tu[1], Jonathan E. McConathy[5], John C. Morris[3,4], Tammie L.S. Benzinger[1,4], and Brian A. Gordon[1,4]

[1]Department of Radiology, Washington University School of Medicine, St. Louis, Missouri; [2]Banner Alzheimer's Institute, Phoenix, Arizona; [3]Department of Neurology, Washington University School of Medicine, St. Louis, Missouri; [4]Charles F. and Joanne Knight Alzheimer Disease Research Center, Washington University School of Medicine, St. Louis, Missouri; and [5]University of Alabama at Birmingham, Birmingham, Alabama

Off-target binding of [^{18}F]flortaucipir (FTP) can complicate quantitative PET analyses. An underdiscussed off-target region is the skull. Here, we characterize how often FTP skull binding occurs, its influence on estimates of Alzheimer disease pathology, its potential drivers, and whether skull uptake is a stable feature across time and tracers. **Methods:** In 313 cognitively normal and mildly impaired participants, CT scans were used to define a skull mask. This mask was used to quantify FTP skull uptake. Skull uptake of the amyloid-β PET tracers [^{18}F]florbetapir and [^{11}C]Pittsburgh compound B (n = 152) was also assessed. Gaussian mixture modeling defined abnormal levels of skull binding for each tracer. We examined the relationship of continuous bone uptake to known off-target binding in the basal ganglia and choroid plexus as well as skull density measured from the CT. Finally, we examined the confounding effect of skull binding on pathologic quantification. **Results:** We found that 50 of 313 (~16%) FTP scans had high levels of skull signal. Most were female (n = 41, 82%), and in women, lower skull density was related to higher FTP skull signal. Visual reads by a neuroradiologist revealed a significant relationship with hyperostosis; however, only 21% of women with high skull binding were diagnosed with hyperostosis. FTP skull signal did not substantially correlate with other known off-target regions. Skull uptake was consistent over longitudinal FTP scans and across tracers. In amyloid-β–negative, but not –positive, individuals, FTP skull binding impacted quantitative estimates in temporal regions. **Conclusion:** FTP skull binding is a stable, participant-specific phenomenon and is unrelated to known off-target regions. Effects were found primarily in women and were partially related to lower bone density. The presence of [^{11}C]Pittsburgh compound B skull binding suggests that defluorination does not fully explain FTP skull signal. As signal in skull bone can impact quantitative analyses and differs across sex, it should be explicitly addressed in studies of aging and Alzheimer disease.

Key Words: off-target binding; human; tau PET; amyloid PET

J Nucl Med 2023; 64:287–293
DOI: 10.2967/jnumed.122.263948

Accrual of hyperphosphorylated tau protein into neurofibrillary tangles is a key pathologic feature of Alzheimer disease (AD) and is significantly predictive of clinical symptomology, cognitive impairment, and neuronal loss (*1*). The most prominent in-human tau PET radiotracer in use is the 5H-pyrido[4,3-b]indole derivative [^{18}F]flortaucipir (FTP, also known as [^{18}F]AV-1451). In vivo use has identified notable off-target FTP binding in the choroid plexus (*2*), basal ganglia, and brain stem (*3*), none of which are believed to have prominent AD-related tauopathy. Possible explanations for this off-target signal include FTP binding to neuromelanin-containing cells (*3*), monoamine oxidase enzymes (*4*), or iron (*2*).

Another off-target region seldom discussed, but nonetheless identified, is skull bone (*5*). The first-in-humans FTP study showed skull uptake in 2 participants (a healthy control and a mild cognitive impairment patient), though this observation was not directly referenced (*6*). Since then, skull signal has been observed anecdotally but minimally noted in the literature. Smith et al. (*7*) recently reported off-target binding in a mask that extended omnidirectionally from the cerebral surface that included meninges, skull bone, and midbrain structures. Although informative, the analyses were limited by the lack of mask specificity and restriction to only amyloid-negative individuals instead of individuals across the AD spectrum. Additionally, whereas they examined data across 3 different tau PET radiotracers, data from only 1 tracer were available for each participant.

High skull binding could adversely impact quantification of AD tauopathy. In the current study, we determined the existence and characteristics of off-target FTP skull binding in cognitively normal adults and those with mild dementia using a subject-specific CT-derived skull region of interest (ROI). We then investigated its impact on quantitative PET analyses and examined its stability using longitudinal FTP scans as well as comparisons with [^{18}F]florbetapir (FBP, also known as [^{18}F]AV-45) and [^{11}C]Pittsburgh compound B (PiB).

MATERIALS AND METHODS

Participants

Data from 313 (177 women/196 men; median age, 69.9 y; age range, 46.2–91.9 y) cognitively normal (n = 273, Clinical Dementia Rating = 0) and impaired individuals (n = 40, Clinical Dementia Rating > 0 and clinical diagnosis of AD dementia or dementia of unknown etiology) enrolled in studies of memory and aging at the Charles F. and Joanne Knight Alzheimer Disease Research Center at Washington University were included in the present study. All participants received FTP and FBP scans within a 1-y period (51.25 ± 63.32 d [mean ± SD]). A subset

Received Feb. 22, 2022; revision accepted Aug. 11, 2022.
For correspondence or reprints, contact Brian A. Gordon (bagordon@wustl.edu).
Published online Aug. 11, 2022.

(n = 14) received longitudinal FTP scans and another subset (n = 152) received a PiB scan in the years before or after the FTP (1,222.74 ± 562.79 d). Clinical and demographic data collected within 1 y from the FTP were also used. The Washington University Institutional Review Board approved all procedures. Written informed consent was obtained from all participants or their designated representatives.

MRI

T1-weighted magnetization-prepared rapid gradient-echo MR images were acquired in sagittal orientation for 176 slices on either a 3-T Biograph PET/MR, Trio, or Vida scanner (Siemens Healthcare). The PET/MRI and Vida scanners used similar parameters (repetition time, 2,300 ms; echo time, 2.95 ms; flip angle, 9°; voxel resolution, 1.05 × 1.05 × 1.19 mm); however, the Trio was slightly modified (repetition time, 2,400 ms; echo time, 3.16 ms; flip angle, 8°; voxel resolution, 1.0 × 1.0 × 1.0 mm). MR images were segmented into ROIs using FreeSurfer (version 5.3-HCP; Martinos Center of Biomedical Imaging).

PET Imaging

Radiotracers were synthesized under current good manufacturing practices and underwent quality assessment and acceptance testing for in-human use before injection. FTP radiochemical purity was reported at 99.9% ± 0.07% over 224 synthesized batches used in the study. As FTP purity was at the ceiling, it was not included in any analyses. For tau PET, participants received a single 339.29 ± 32.93 MBq intravenous bolus of FTP. Emission data were collected for the 0- to 110-min (n = 117) or 80- to 100-min (n = 196) postinjection time interval (p.t.i.) on a Siemens Biograph PET/CT scanner. List-mode data were reconstructed using ordered-subset expectation maximization with no postreconstruction filtering and standard normalization, decay and scatter correction, and dead time. CT transmission scans detailing bone structure and tissue were also obtained.

Amyloid PET was performed with either FBP or PiB on a Siemens Biograph PET/MR scanner or a Biograph PET/CT scanner. After a single bolus injection of 370 ± 22.2 MBq of FBP, emission data covered the p.t.i. of 0–70 (n = 210) or 50–70 min (n = 103); for PiB, 513.56 ± 128.02 MBq were administered, with data covering the p.t.i. of 0–60 (n = 150) or 30–60 min (n = 2). For data collected on the PET/MRI scanner, separate CT images were obtained to generate a CT-based μmap for attenuation correction (*8*). Reconstruction procedures were similar to those for tau PET.

PET data were analyzed using the FreeSurfer-based PET Unified Pipeline (https://github.com/ysu001/PUP), which includes scanner resolution harmonization (*9*), interframe motion correction, PET-to-MRI registration, ROI-based time–activity curve extraction, SUV ratio (SUVr) analyses, geometric transfer matrix–based partial-volume correction (PVC) (*10*), and a non-PVC voxelwise SUVr image coregistered to the structural MRI. SUVrs were calculated for the 80- to 100-, 50- to 70-, and 30- to 60-min p.t.i. for FTP, FBP, and PiB, respectively. Cerebellar gray matter served as the reference region regardless of tracer. Global amyloid burden was calculated as the average of PVC SUVrs for the prefrontal, inferior temporal, precuneal, and gyrus rectus regions. Positivity was based on published values of 1.42 for PiB (*11*) and 1.19 in FBP (*12*). Regional PVC FTP SUVrs for the amygdala, entorhinal, inferior temporal, and lateral occipital were averaged into a tauopathy summary measure (*13*).

Skull ROI

To create an individual-specific skull ROI, each CT image was linearly aligned using the FMRIB Linear Image Registration Tool with its respective T1 image, which in turn was coregistered to the Montreal Neurological Institute (MNI)–152 stereotactic atlas. The MNI-aligned CT images were then averaged across the cohort. On this population average, a mask of nonskull structures (e.g., vertebra and muscles) was generated using the fslmaths and FSLeyes utilities and then removed from the averaged CT image. Voxels below 1,400 Hounsfield units were also removed so that only dense cranial bone remained. The image was then inflated twice using a 2-mm gaussian kernel to capture the largest possible skull size and then nonzero voxels binarized at a threshold of 0.1 Hounsfield units. This mask was then placed back into subject space and applied to the participant's original binarized CT image to generate an individual skull ROI with nonskull structures removed (Fig. 1). The skull ROI was then applied to each voxelwise non-PVC SUVr image, and skull uptake was calculated as the average SUVr within the ROI.

Visual Reads

All CT images were visually inspected by 1 of 2 neuroradiologists who had a combined 17 y of experience and did not know our hypotheses. The assessment included identifying hyperostosis cranialis interna (a hereditary disease of the skull and sphenoid bone) and sinusitis, as well as an open-ended identification of other bone or skull abnormalities deemed significant. No participants were excluded because of incidental findings.

Statistical Analysis

Analyses were performed using R software (version 3.3.2, R Core Team). After the skull SUVr had been computed, participants were classified as either having low (S−) or high (S+) skull binding using a gaussian mixture model with 2 components from the mclust package (version 5.3) (*14*). Participants were further subdivided by amyloid positivity (A+/−) based on global amyloid burden. Demographic differences were assessed using Welch t tests for continuous variables and Fisher exact tests for categoric variables because of the small size of some groups. Skull SUVr from doses split between individuals scanned on the same day were evaluated using a Pearson correlation. To investigate the possibility of asymmetric FTP binding in the skull, we divided the skull ROI across its midline, obtained SUVrs for both left and right portions, and then assessed the relationship between left and right skull using a Pearson correlation.

We first tested whether skull SUVr shared variance with known FTP off-target regions using partial correlations controlling for age, as well as linear models with main effects of skull SUVr, age, sex, and a sex-by-skull SUVr interaction. Sex was selected as a factor because of previously identified sex differences in FTP skull binding (*7*). We then examined whether bone density, calculated as the average Hounsfield units in the acquired CT scan, influenced skull SUVr using a linear model with a main effect of sex and a sex–by–cranial-bone density interaction. Results from the CT image visual reads were evaluated using Fisher exact tests.

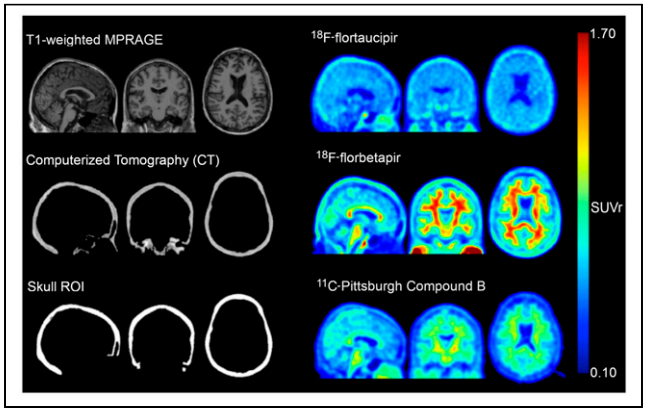

FIGURE 1. MR, CT, and SUVr images from amyloid-negative participant with high skull binding in all 3 radiotracers. Images are in MNI-152 space. MPRAGE = magnetization-prepared rapid acquisition with gradient echo.

To determine FTP skull signal's impact on quantitative PET, linear regression and partial correlations controlling for age assessed whether skull SUVr and the tauopathy summary measure differed as a function of amyloid status. Further analyses used linear models predicting regional SUVr from skull SUVr with P values adjusted for multiple comparisons using the Benjamini–Hochberg procedure at a false discovery rate of $q = 0.05$. Similar models were run that included main effects of age and sex.

Spearman correlations tested the radioisotope specificity of skull SUVr between FTP and the 2 amyloid tracers (FBP and PiB) in the same participants. As with FTP, we examined asymmetric FBP and PiB skull binding using a Pearson correlation. We further plotted the mean time–activity curves for several ROIs, including skull, for each tracer. Finally, longitudinal stability of skull binding was assessed with a Pearson correlation between baseline and a randomly chosen follow-up visit in those with longitudinal data.

RESULTS

FTP Skull Binding Characteristics

Group-average FTP SUVr images based on amyloid positivity as well as skull binding levels (A+/−, S+/−) are shown in Figure 2. Exemplar cases of high skull binding are shown in Supplemental Figure 1 (supplemental materials are available at http://jnm.snmjournals.org), and demographic information is in Table 1. Women were more likely to be classified S+ than men ($\chi^2_1 = 18.19$, $P < 0.001$) but were equally likely to be classified A+/− ($\chi^2_1 = 0.08$, $P = 0.77$). Women composed the majority of the S+ group, regardless of amyloid status (83.8% for S+/A− and 76.9% for S+/A+). S+ individuals were typically younger ($t_{67.45} = 3.55$, $P < 0.001$) than their S− counterparts. There was no association for skull SUVr between individuals who received injections from the same synthesized FTP batch ($n = 179$, $r = 0.07$, $P = 0.44$). FTP SUVrs between the left and right portions of the skull correlated significantly ($r = 0.98$, $P < 0.001$; Supplemental Fig. 2).

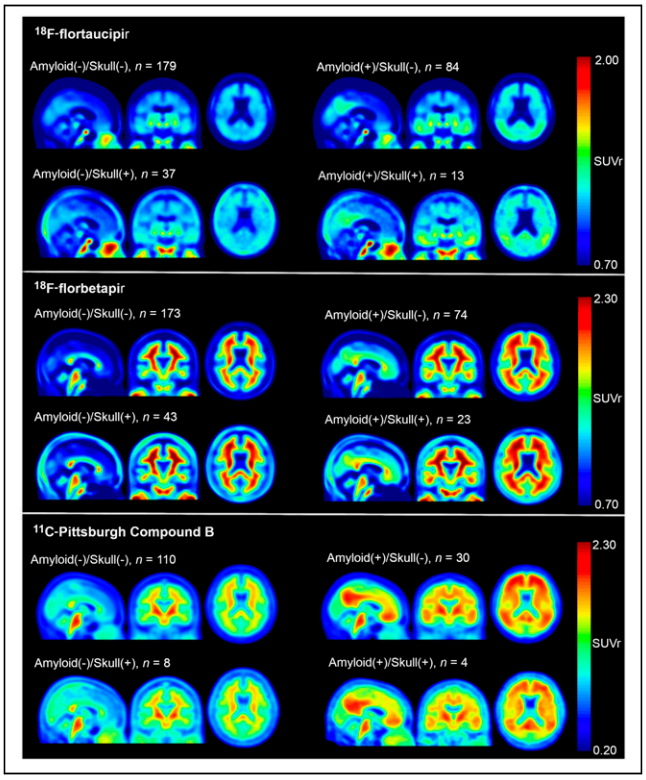

FIGURE 2. Group average SUVr images for each tracer. Images are in MNI-152 space.

TABLE 1
Demographics for FTP Groups

Demographic	*n*	High skull binding	Low skull binding	*P**
Sex	313			<0.001
Female		42 (84%)	135 (51%)	
Male		8 (16%)	128 (49%)	
Age (y)	312			<0.001
Mean		66	70	
SD		8	8	
Education (y)	299			0.60
Mean		15.85	16.03	
SD		2.11	2.30	
Clinical dementia rating	313			0.68
0		46 (92%)	227 (86%)	
0.5		3 (6.0%)	29 (11%)	
≥1		1 (2.0%)	7 (2.7%)	
MMSE	311			0.87
Mean		28.92	28.86	
SD		2.51	1.91	
Amyloid status	313			0.51
Negative		37 (74%)	179 (68%)	
Positive		13 (26%)	84 (32%)	

*Differences assessed using Welch 2-sample *t* tests and Fisher exact tests.
MMSE = Mini-Mental State Examination.

Lack of Relationship Between FTP Skull Binding and Other Off-Target Regions

FTP skull SUVr was not related to choroid plexus binding (partial correlation: $r = 0.004$, $P = 0.93$; Fig. 3A). A linear model predicting choroid plexus SUVr found no effects of skull SUVr ($t_{308} = 0.03$, $P = 0.98$), sex ($t_{308} = -0.11$, $P = 0.90$), or age ($t_{308} = -0.48$, $P = 0.63$). Additionally, the sex-by-skull SUVr interaction was not significant ($t_{308} = 0.18$, $P = 0.86$). Repeating the analysis using PVC SUVr yielded similar results except that increased age showed higher choroid plexus PVC SUVrs ($t_{308} = 2.90$, $P < 0.01$); however, this effect has already been noted (*15*). Skull SUVr was negatively associated with basal ganglia SUVr (partial correlation: $r = -0.14$, $P = 0.01$; Fig. 3B) such that basal ganglia SUVr decreased with increasing skull SUVr. The linear model evaluating basal ganglia FTP signal found an effect of age ($t_{308} = 6.05$, $P < 0.001$) but no effect of skull SUVr ($t_{308} = -1.71$, $P = 0.09$), sex ($t_{308} = 0.95$, $P = 0.34$), or interaction between sex and skull SUVr ($t_{308} = -1.32$, $P = 0.19$). Repeating the analysis using PVC SUVr produced similar results.

Relationship Between Decreased Cranial Bone Density and FTP Skull Uptake in Women

A linear model predicting FTP skull SUVr found main effects of sex ($t_{309} = -3.10$, $P < 0.01$) and bone density ($t_{309} = -6.64$,

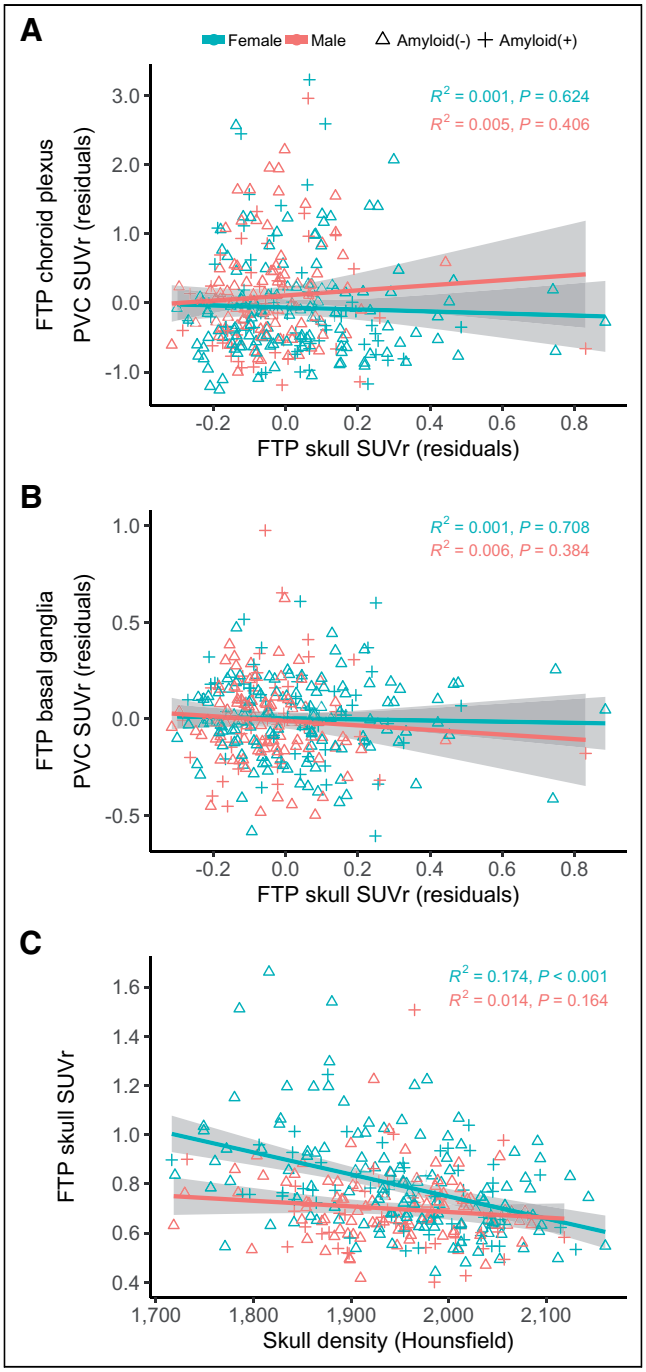

FIGURE 3. (A and B) Partial correlations of FTP skull SUVr with FTP choroid plexus partial-volume–corrected (PVC) SUVr (A) and FTP basal ganglia PVC SUVr (B) for men and women. (C) Women with lower bone density displayed higher skull SUVrs, whereas men did not. Shaded regions are 95% CIs.

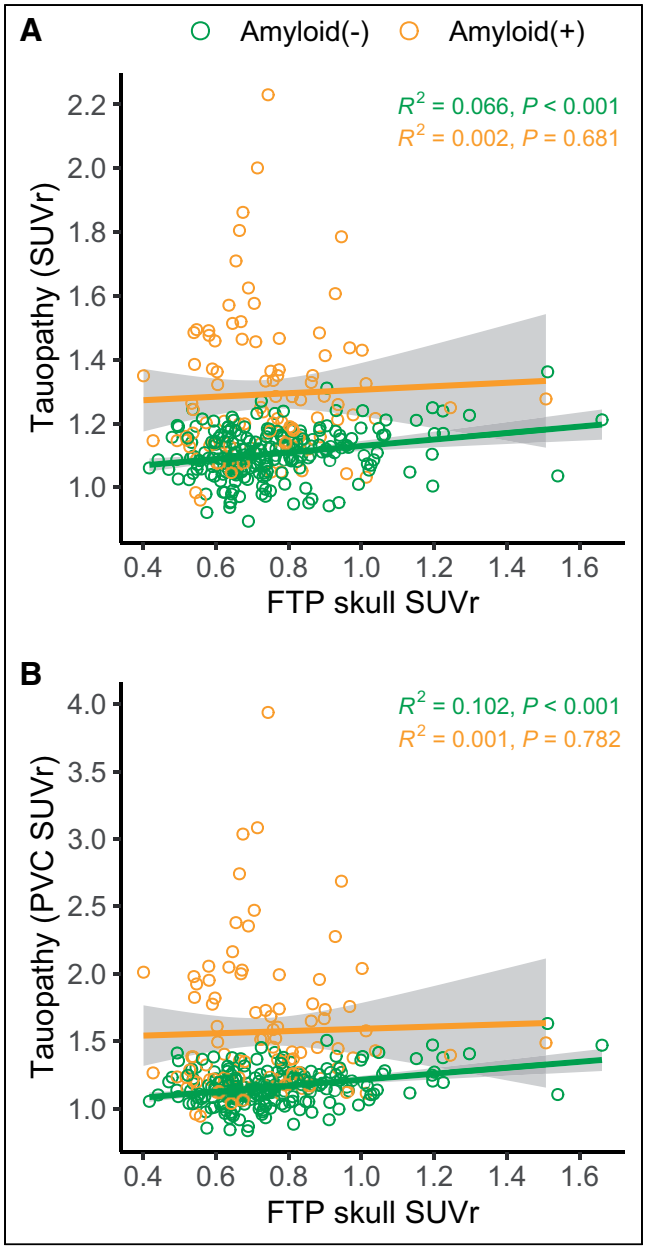

FIGURE 4. Relationship between FTP skull SUVr and tauopathy summary measure without (A) and with (B) PVC. Shaded regions are 95% CIs.

$P < 0.001$), as well as a significant interaction ($t_{309} = 2.89$, $P < 0.01$; Fig. 3C). When stratified by sex, women had a significant negative association in which those with decreased skull density displayed higher skull SUVr ($t_{175} = -6.08$, $P < 0.001$) whereas men did not ($t_{134} = -1.40$, $P = 0.16$). Clinical assessments of CT images revealed 33 participants with hyperostosis (20 S−/13 S+). We found a significant relationship between skull binding and a hyperostosis diagnosis ($P < 0.001$). Approximately 21% (9/42) of S+ women and 50% (4/8) of S+ men were positive for hyperostosis. The visual reads also revealed 20 participants with sinusitis (16 S−/4 S+), although this was unrelated to skull binding ($P = 0.54$). No other significant bone abnormalities were identified.

Impact of FTP Skull Binding on Quantitative PET

FTP skull SUVr correlated with the tauopathy summary measure in A− (partial correlation: $r = 0.32$, $P < 0.001$) but not A+ individuals (partial correlation: $r = 0.06$, $P = 0.58$; Fig. 4; Supplemental Fig. 3). The correlation observed in A− may be explained by possible bleed-over from proximal skull. Regional impacts of skull binding are shown in Figure 5. In A− individuals, increased skull SUVr produced significantly elevated regional non-PVC SUVrs in the frontal, parietal, and temporal lobes, whereas in A+ individuals, only the postcentral and pars orbitalis non-PVC SUVr

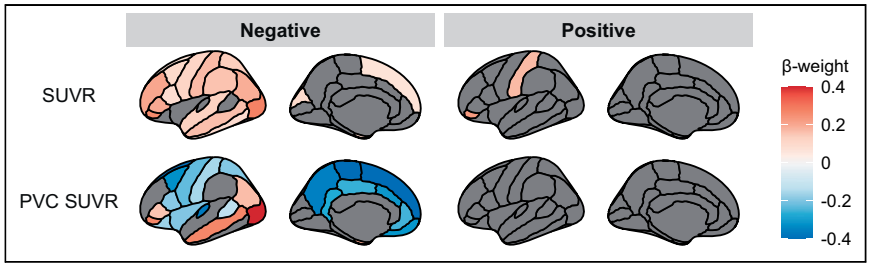

FIGURE 5. Cortical regions significantly associated ($P < 0.05$) with FTP skull partial-volume–corrected (PVC) SUVr and non-PVC SUVr for amyloid-negative and -positive individuals.

showed any relationship with skull SUVr. After application of regional PVC, in A− individuals only the middle temporal, inferior parietal, and lateral occipital continued to show elevated regional PVC SUVr. All other previously significant regions either inverted or did not survive multiple-comparisons correction. For A+ individuals, no regions showed a relationship with skull SUVr. Similar analyses controlling for sex and age are in Supplemental Figure 4.

Skull Binding in Amyloid PET

As with FTP, participants were grouped as S+/− using a gaussian mixture model and further grouped into A+/− on the basis of the respective amyloid tracer. Demographics are in Supplemental Table 1 for FBP and Supplemental Table 2 for PiB, and group-average SUVr images are shown in Figure 2. Sex was related to FBP skull SUVr in both A− ($\chi^2_1 = 37.64$, $P < 0.001$) and A+ individuals ($\chi^2_1 = 10.44$, $P = 0.001$), with women composing 97.6% and 86.9% of the S+ groups, respectively. Although sex was not significant for PiB, few individuals were classified as S+ (8/118, 7%). When examined as a continuous measure, skull SUVr from both tracers significantly correlated with FTP skull SUVr (FBP: $\rho = 0.48$, $P < 0.001$; PiB: $\rho = 0.34$, $P < 0.001$; Figs. 6A and 6B). Mean time–activity curves are presented in Supplemental Figure 5. Generally, skull signal appeared relatively constant, with minimal decay relative to other ROIs in all 3 tracers. SUVrs between left and right skull correlated significantly for both FBP ($r = 0.98$, $P < 0.001$) and PiB ($r = 0.96$, $P < 0.001$; Supplemental Fig. 2).

Longitudinal Stability of FTP Skull Binding

Using our longitudinal FTP data, skull SUVr at baseline correlated significantly with that at follow-up ($r = 0.84$, $P < 0.001$; Fig. 6C). An exemplar longitudinal case with high skull binding is shown in Supplemental Figure 6.

DISCUSSION

Previous studies evaluating FTP have noted off-target binding in subcortical regions as well as the skull. Although binding in subcortical regions has been investigated, skull binding has largely been ignored. In a cohort of nondemented older adults and those with mild dementia, we found that 15.9% of individuals scanned with FTP showed elevated skull signal and that this binding influenced estimates of tau pathology in the temporal lobe. Further, skull binding is a stable, individual-specific property tied to sex.

The biologic drivers behind bone uptake are unknown, but the current work reveals important insights. The longitudinal analyses demonstrate that skull binding was consistent across time points, whereas the multitracer analyses suggest that relative levels of skull binding were consistent across FTP, FBP, and PiB. This finding indicates that individuals with elevated skull binding for 1 tracer and time point are likely to have elevated binding at subsequent visits. In the literature, skull signal is usually attributed to spontaneous defluorination of the ^{18}F-fluorine radioisotope (*16*). The significant predicative relationship between clinically diagnosed hyperostosis and skull binding would appear to support this claim. However, we also found that PiB skull SUVr was linearly related to FTP skull SUVr in the same individuals, though the number of PiB individuals classified as S+ was low compared with FTP and FBP. These findings suggest that other factors beyond purely defluorination may be involved in the presence of skull signal. The high FTP radiochemical purity also suggests that skull binding is unlikely to be due to factors involved in radiotracer synthesis.

Elevated binding is driven primarily by the female sex, a finding also observed by Smith et al. (*7*) in tau PET using FTP, ^{18}F-MK-6240, and ^{18}F-RO948. In the present study, women with higher FTP skull binding had low bone density as measured by CT. Women often experience a greater decline in bone density with age than men, including in the cranium (*17*); our findings support the theory that bone loss is at least partially driving skull binding but is not simply age-related, as overall bone density did not significantly change with increased age for either sex (Supplemental Fig. 7). Recent work with 18-kDa translocator protein tracers in participants with central nervous system disorders found a relationship between decreasing bone density and skull signal in women. These results suggest a role of inflammatory processes and alterations in bone marrow structure (*18*). Future work should directly compare 18-kDa translocator protein and tau PET skull binding to explore this possibility.

Bone uptake was also distinct from choroid plexus binding, although a negative relationship was present for the basal ganglia. It has been speculated that basal ganglia signal is tied to iron (*19*), and there are reports of sex-related differences in iron accumulation in the brain (*20*); such a connection should be explored in future work. The negative association with the basal ganglia may also be tied to age, as FTP in the basal ganglia increases with age, whereas we found that it was a subset of relatively younger, rather than older, women that was driving the observed skull uptake.

The temporal cortex has consistently been shown to have an elevated tau PET signal in both the prodromal (*21*) and the clinical phases of AD (*1*). Our analyses demonstrated that in amyloid-negative individuals, bone uptake was positively related to tau PET signal in the inferior temporal cortex and that applying regional PVC partially mitigated these effects. Spillover from bone could spuriously elevate measurements in some individuals and reduce concordance between multiple tauopathy measures. It may also limit the sensitivity of tau PET tracers to increases in true pathology during the early phases of AD. The strong sex effect observed suggests that bone binding should be considered, particularly in investigations of sex on tau PET (*22–24*).

Our multitracer comparisons indicated that individuals with high bone signal in one tracer are likely to have elevated signal with another tracer. SUVrs were quite high for FTP (0.751 ± 0.187) and FBP (0.885 ± 0.200) but were at a lower range for PiB (0.572 ± 0.087), indicating that this off-target binding is not tied

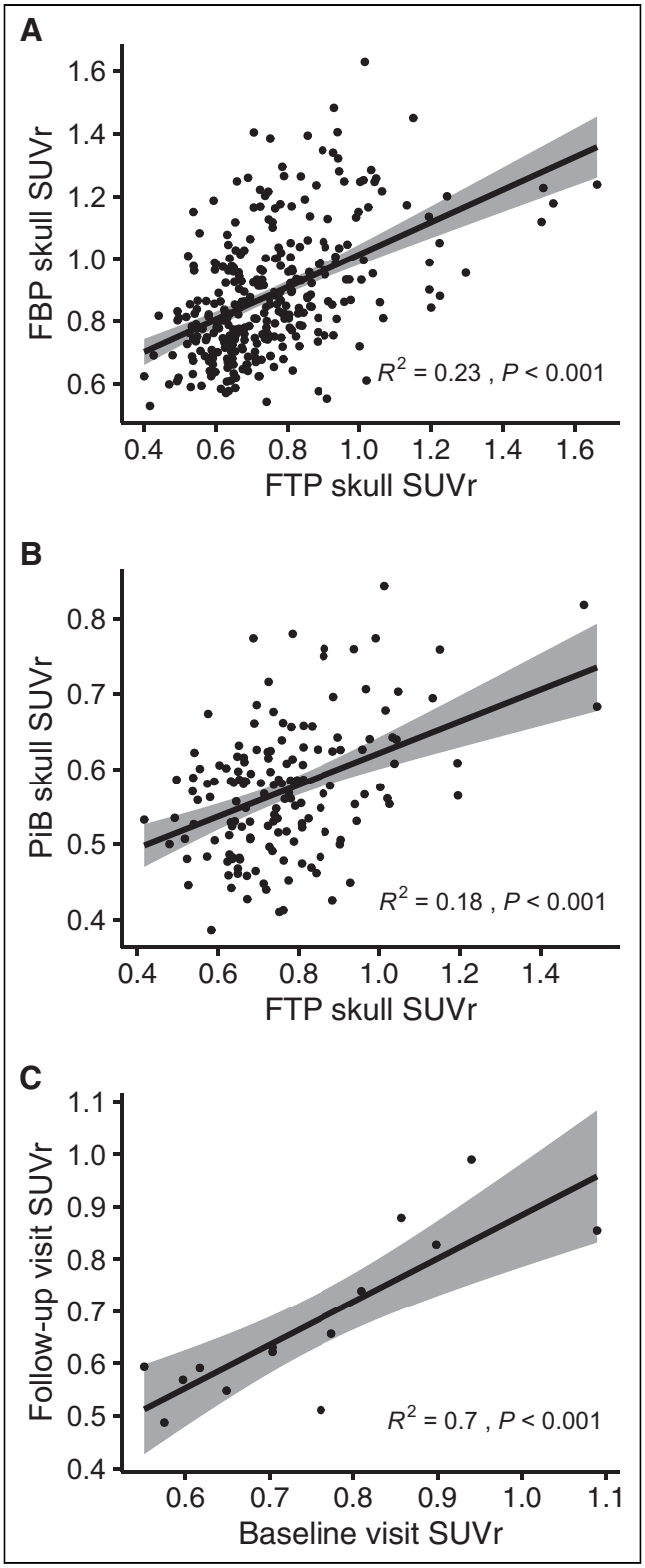

FIGURE 6. (A and B) Multitracer comparisons between FTP skull SUVr and FBP (A) or PiB (B) skull SUVr. (C) Longitudinal relationship for skull uptake across FTP visits. Shaded regions are 95% CIs.

to target receptor (e.g., tangles vs. plaques) but that the radioisotope (^{18}F vs. ^{11}C) determines the degree of bone uptake. Alternatively, the time–activity curves suggest that bone signal appears constant, whereas counts in brain tissue continue to fall at later time points. Consequently, tracers with a later p.t.i. (i.e., FTP and FBP) are more likely to see problematic contamination. Future work with additional tracers could clarify what factors modulate the degree of skull binding.

There are several limitations to the current study. First, as the PiB scan dates were not constrained to within a certain time frame from FTP, we could not fully investigate age-related factors of skull binding. Additionally, comprehensive participant medical histories were not available, limiting investigations into the role, if any, of medication (e.g., hormone replacement therapy) and medical condition; however, Smith et al. (*7*) found no relationship with either. Lastly, our analyses were limited to a single cohort. Future work should extend the presented analyses to other cohorts to elucidate the frequency of FTP skull binding across multiple longitudinal studies and the biologic factors that influence its presentation.

CONCLUSION

FTP skull binding occurred in 15.9% of a sample of cognitively normal adults and those with mild dementia, and this effect was overwhelmingly observed in women. Increased binding was a stable feature across time and multiple tracers. In individuals without amyloid pathology, skull uptake led to elevated tau SUVrs in regions thought to be tied to AD. This could potentially hamper the early detection of emerging tau pathology and merits further investigation.

DISCLOSURE

This research was supported by NIH grants P30AG66444, P01AG003991, P01AG026276, U01AG042791, R01AG046179, R01AG055444, and R01AG031581. Image acquisition and analysis received additional support from UL1TR000448, P30NS098577, and R01EB009352. Additional support was provided by the Arizona Alzheimer's Research Consortium, the Charles and Joanne Knight Alzheimer Disease Research Center Support Fund, the David and Betty Farrell Medical Research Fund, the Daniel J. Brennan Alzheimer Research Fund, the Fred Simmons and Olga Mohan Alzheimer Research Support Fund, the Barnes–Jewish Hospital Foundation, Eli Lilly & Co., Hoffman La-Roche, Avid Radiopharmaceuticals, the Alzheimer's Association, the GHR Foundation, and an anonymous organization. Avid Radiopharmaceuticals provided the FBP doses, assisted with scanning expenses, and provided precursor and technology transfer for FTP. Manu Goyal reports trip reimbursement and honoraria in 2019 from sponsors of the Linyi Brain PET conference, including Capital Medical University, Tancheng Talent Office, and Shandong Madic Technologies Co., Ltd., and stock equity in IBM, Moderna, and BioNTech. Dean Wong reports investigator-initiated funding from the National Institutes of Health (NIH) and contracts to John Hopkins University and Washington University from LB Pharma, Eisai, Roche Neuroscience, Anavex, Five Eleven Pharma, and Lundbeck (Denmark/US). Tammie Benzinger reports investigator-initiated funding from the NIH, the Alzheimer's Association, the Barnes–Jewish Hospital Foundation, and Avid Radiopharmaceuticals; participates as a site investigator in clinical trials sponsored by Avid Radiopharmaceuticals, Eli Lilly, Biogen, Eisai, Jaansen, and Roche; serves as an unpaid consultant to Eisai and Siemens; and is on the speakers' bureau for Biogen. No other potential conflict of interest relevant to this article was reported.

KEY POINTS

QUESTION: What are the characteristics and quantitative impacts of FTP skull signal?

PERTINENT FINDINGS: We examined FTP skull signal in a cohort of cognitively unimpaired adults and those with mild dementia using a skull mask derived from their own CT scan. Skull signal was observed primarily in younger women with decreased skull bone density, was a stable feature across time and tracers, and erroneously elevated quantitative measures of early tau accumulation in AD.

IMPLICATIONS FOR PATIENT CARE: FTP skull signal should be considered in examining early increases in tau pathology in neurologic PET studies.

REFERENCES

1. Brier MR, Gordon B, Friedrichsen K, et al. Tau and Ab imaging, CSF measures, and cognition in Alzheimer's disease. *Sci Transl Med.* 2016;8:338ra66.
2. Choi JY, Cho H, Ahn SJ, et al. Off-target ^{18}F-AV-1451 binding in the basal ganglia correlates with age-related iron accumulation. *J Nucl Med.* 2018;59:117–120.
3. Lowe VJ, Curran G, Fang P, et al. An autoradiographic evaluation of AV-1451 tau PET in dementia. *Acta Neuropathol Commun.* 2016;4:58.
4. Barrio JR. The irony of PET tau probe specificity. *J Nucl Med.* 2018;59:115–116.
5. Smith R, Schöll M, Leuzy A, et al. Head-to-head comparison of tau positron emission tomography tracers [^{18}F]flortaucipir and [^{18}F]RO948. *Eur J Nucl Med Mol Imaging.* 2020;47:342–354.
6. Chien DT, Bahri S, Szardenings AK, et al. Early clinical PET imaging results with the novel PHF-tau radioligand [F-18]-T807. *J Alzheimers Dis.* 2013;34:457–468.
7. Smith R, Strandberg O, Leuzy A, et al. Sex differences in off-target binding using tau positron emission tomography. *Neuroimage Clin.* 2021;31:102708.
8. Su Y, Rubin BB, McConathy J, et al. Impact of MR-based attenuation correction on neurologic PET studies. *J Nucl Med.* 2016;57:913–917.
9. Joshi A, Koeppe RA, Fessler JA. Reducing between scanner differences in multi-center PET studies. *Neuroimage.* 2009;46:154–159.
10. Rousset OG, Collins DL, Rahmim A, Wong DF. Design and implementation of an automated partial volume correction in PET: application to dopamine receptor quantification in the normal human striatum. *J Nucl Med.* 2008;49:1097–1106.
11. Su Y, D'Angelo GM, Vlassenko AG, et al. Quantitative analysis of PiB-PET with FreeSurfer ROIs. *PLoS ONE.* 2013;8:e73377.
12. Su Y, Flores S, Wang G, et al. Comparison of Pittsburgh compound B and florbetapir in cross-sectional and longitudinal studies. *Alzheimers Dement (Amst).* 2019;11:180–190.
13. Mishra S, Gordon BA, Su Y, et al. AV-1451 PET imaging of tau pathology in preclinical Alzheimer disease: defining a summary measure. *Neuroimage.* 2017;161:171–178.
14. Scrucca L, Fop M, Murphy TB, Raftery AE. Mclust 5: clustering, classification and density estimation using Gaussian finite mixture models. *R J.* 2016;8:289–317.
15. Wen GY, Wisniewski HM, Kascsak RJ. Biondi ring tangles in the choroid plexus of Alzheimer's disease and normal aging brains: a quantitative study. *Brain Res.* 1999;832:40–46.
16. *Amyvid EU Summary of Product Characteristics.* European Medicines Agency; 2013.
17. Schulte-Geers C, Obert M, Schilling RL, et al. Age and gender-dependent bone density changes of the human skull disclosed by high-resolution flat-panel computed tomography. *Int J Legal Med.* 2011;125:417–425.
18. Kolabas ZI, Kuemmerle LB, Perneczky R, et al. Multi-omics and 3D-imaging reveal bone heterogeneity and unique calvaria cells in neuroinflammation. bioRxiv website. https://www.biorxiv.org/content/10.1101/2021.12.24.473988v1. Published December 25, 2021. Accessed November 18, 2022.
19. Spotorno N, Acosta-Cabronero J, Stomrud E, et al. Relationship between cortical iron and tau aggregation in Alzheimer's disease. *Brain.* 2020;143:1341–1349.
20. Persson N, Wu J, Zhang Q, et al. Age and sex related differences in subcortical brain iron concentrations among healthy adults. *Neuroimage.* 2015;122:385–398.
21. Schultz SA, Gordon BA, Mishra S, et al. Widespread distribution of tauopathy in preclinical Alzheimer's disease. *Neurobiol Aging.* 2018;72:177–185.
22. Buckley RF, Scott MR, Jacobs HIL, et al. Sex mediates relationships between regional tau pathology and cognitive decline. *Ann Neurol.* 2020;88:921–932.
23. Wisch JK, Meeker KL, Gordon BA, et al. Sex-related differences in tau positron emission tomography (PET) and the effects of hormone therapy (HT). *Alzheimer Dis Assoc Disord.* 2021;35:164–168.
24. Buckley RF, O'Donnell A, McGrath ER, et al. Menopause status moderates sex differences in tau burden: a Framingham PET study. *Ann Neurol.* 2022;92:11–22.